Journal of ELECTRONIC MATERIALS, Vol. 41, No. 4, 2012
DOI: 10.1007/s11664-012-1943-7

Microstructure Evolution and Defect Formation in Cu Through-Silicon Vias (TSVs) During Thermal Annealing

HAE-A-SEUL SHIN,[1] BYOUNG-JOON KIM,[1] JU-HEON KIM,[2] SUNG-HWAN HWANG,[1] ARIEF SURIADI BUDIMAN,[3] HO-YOUNG SON,[4] KWANG-YOO BYUN,[4] NOBUMICHI TAMURA,[5] MARTIN KUNZ,[5] DONG-IK KIM,[2] and YOUNG-CHANG JOO[1,6]

1.—Department of Materials Science & Engineering, Seoul National University, Seoul, Korea. 2.—Materials Science and Technology Division, Korea Institute of Science and Technology, Seoul, Korea. 3.—Center for Integrated Nanotechnologies (CINT), Los Alamos National Laboratory, Los Alamos, NM, USA. 4.—PKG Development Group, Research & Development Division, Hynix Semiconductor Inc., Icheon, Korea. 5.—Advanced Light Source (ALS), Lawrence Berkeley National Laboratory, Berkeley, CA, USA. 6.—e-mail: ycjoo@snu.ac.kr

The microstructural evolution of Cu through-silicon vias (TSVs) during thermal annealing was investigated by analyzing the Cu microstructure and the effects of twin boundaries and stress in the TSV. The Cu TSV had two regions with different grain sizes between the center and the edge with a random Cu texture before and after annealing. The grain size of large grains was almost unchanged after annealing, and the abrupt grain growth was restricted by the twin boundaries due to their structural stability. However, microvoids and cracks in the Cu TSV were observed after annealing. These defects were formed by the stress concentration among Cu grains. After defects were formed, the stress level of the TSV was decreased after annealing.

Key words: Through-silicon via (TSV), copper, microstructure, twin, stress

INTRODUCTION

The three-dimensional system-in-package (3-D SIP) has emerged as a system enabling high device integration and performance. The chip integration design has changed from long, wired, two-dimensional packaging to short, vertical, three-dimensional stacking.[1–5] Through-silicon via (TSV) technology has received the most attention because this technique offers system design flexibility, low cost, and integration of heterogeneous chips. In addition, TSV has excellent electrical properties, such as high conductivity and low *RC* delay.[6–8]

Cu is the strongest candidate for TSV materials due to its low resistivity; however, some reliability issues are induced by the thermal stress generated due to the large mismatch between the coefficients of thermal expansion for Cu (17.70 ppm/°C) and Si (2.61 ppm/°C) during thermal cycling. TSVs should undergo thermal loading after formation during the integration process. After via etching and filling, TSVs will undergo thermal cycling at 400°C with metallization and/or at 200°C with the bonding process. These thermal cycling procedures during fabrication may induce mechanical failure of TSVs.

The stress level in TSVs and its profile are important for TSV reliability. To predict and measure the stress level, several researchers have studied the stress level with simulations using finite-element modeling and with experimental techniques such as μ-Raman spectroscopy, x-ray diffraction, and digital image speckle correlation.[9–11] In addition to stress, the microstructural evolution of the Cu grains in TSVs is important for understanding the stress profile and controlling its level, because microstructural variation is the origin of stress. Furthermore, the microstructure of Cu TSVs may change with grain growth, or damage may occur during thermal processing. The possible defects include voids and cracks in the interior of the TSV and extrusion of Cu outside of the TSV.

(Received September 8, 2011; accepted January 17, 2012; published online February 17, 2012)

These microstructural changes are affected by aspects of the microstructure, such as texture, grain boundaries, or a twin boundary. Therefore, the microstructural evolution in TSVs during thermal cycling is important for TSV reliability, and understanding of the microstructural evolution, along with understanding of the microstructural characteristics and inherent stress before and after annealing, is essential for reliable 3-D packaging.

The microstructure of Cu TSVs has been reported with scanned images obtained using optical microscopy, scanning electron microscopy, and focused ion beam (FIB) techniques, but only after fabrication optimization.[12–16] Recently, Okoro et al. reported that no preferred texture and grain growth were observed in Cu TSVs under various annealing conditions with FIB and electron backscatter diffraction (EBSD) results.[17] However, this report focused on analyzing the results of hardness and elastic modulus with grain size and residual stress. An in-depth study on the microstructural evolution or defects in the TSV was not reported.

In this study, the microstructural characteristics and evolution on annealing of Cu TSVs were studied from the perspective of the effect of twin boundaries and formation of defects, such as voids and cracks, using FIB images and EBSD data. Furthermore, the relationship between mechanical stress and microstructure is discussed based on the results of synchrotron x-ray microdiffraction measurements.

EXPERIMENTAL PROCEDURES

A TSV sample with 20 μm diameter and 90 μm height was prepared. After metallization, vias were prepared by deep reactive-ion etching and a silicon oxide layer and a titanium barrier material were deposited on the via walls. Cu was then electroplated at current density of 10 A/m^2 for 10 min and at 100 A/m^2 for 60 min. This type of sample was not annealed after TSV formation because the process of TSV formation was the so-called via-last process. For the via-last process, in which TSV is formed after back end of the line (BEOL), the TSV will be treated at 200°C with a bonding process. After fabrication, the bonding process will be applied, therefore TSVs may be subject to thermal loading at 200°C during the bonding process for 3-D packaging.

To study the effects of annealing on the microstructure of Cu TSV, thermal annealing was conducted at 200°C for 1 h with 13.3×10^{-5} Pa vacuum condition and ramping rate of about 4.5°C/min. The samples were allowed to cool before being taken out of the furnace. This condition was chosen because thermal loading at 200°C is inevitable for via-last TSVs due to the bonding process in wafer integration. To study the effects of aging on microstructural variation, the TSV sample was aged for 1 year at room temperature.

The microstructural characteristics of the Cu TSV were analyzed by FIB and EBSD both before and after annealing. For FIB analysis, milling and scanning were conducted by a Ga-ion source in the FIB. An ion miller with an Ar gas source was used for surface refinement for sample preparation for EBSD measurements.

Stress measurements were performed by synchrotron x-ray microdiffraction at beamline 12.3.2 at the Advanced Light Source of Lawrence Berkeley National Laboratory. A schematic figure and the method of stress calculation for deviatoric stress and hydrostatic stress are presented in Fig. 1. The energy range of the x-ray beam of this beamline is approximately 5 keV to 24 keV, and the beam comes from a bending magnet, providing a continuous energy distribution. The x-ray beam was focused by Kirkpatrick–Baez (KB) mirrors, and diffraction data were collected using an MAR133 charge-coupled device (CCD) camera.[18] Synchrotron x-ray microdiffraction has a 1 μm $\times$ 1 μm beam size, allowing the local stress of specific positions of interest to be measured. The stress was measured for every 1 μm $\times$ 1 μm area in the TSV sample. The total strain tensor was obtained from the sum of the deviatoric components obtained by analyzing the Laue pattern and the hydrostatic (dilatational) components obtained by energy scanning. The hydrostatic stress was measured using a monochromatic beam, and energy scanning was conducted from 9.8 keV to 10.2 keV in 0.1-keV steps. Stress measurements were performed before annealing and after fully cooling from 200°C to room temperature. The diffraction patterns were analyzed by x-ray microdiffraction analysis (XMAS) software developed in-house for beamline 12.3.2.

RESULTS AND DISCUSSION

Figure 2 shows FIB images of the TSVs and compares the microstructure of the TSVs. Figure 2a shows the TSV before annealing, and Fig. 2b shows the TSV after annealing. Before annealing, the Cu TSV had large grains in the center of the TSV and small grains at the top and sides of the TSV. After annealing, the TSV had both small grains and large grains; however, the large-grain region was enlarged, and the portion of fine grains was reduced with some remaining at the top and side of the TSV. The regions between the small-grained area and the large-grained area are separated by a dotted line in Fig. 2.

The size deviation among the grains in the TSV was exacerbated by the electroplating process during the TSV formation, and this phenomenon was observed in the case of the Cu films or the Cu vias formed by electroplating (depending on the deposition conditions).[19,20] Because small grains were less stable than large grains, grain growth of the small grains occurred during thermal treatment. However, not all of the small grains had grown after 1 h of annealing at 200°C, and the sample maintained overall the two regions distinguished by the grain

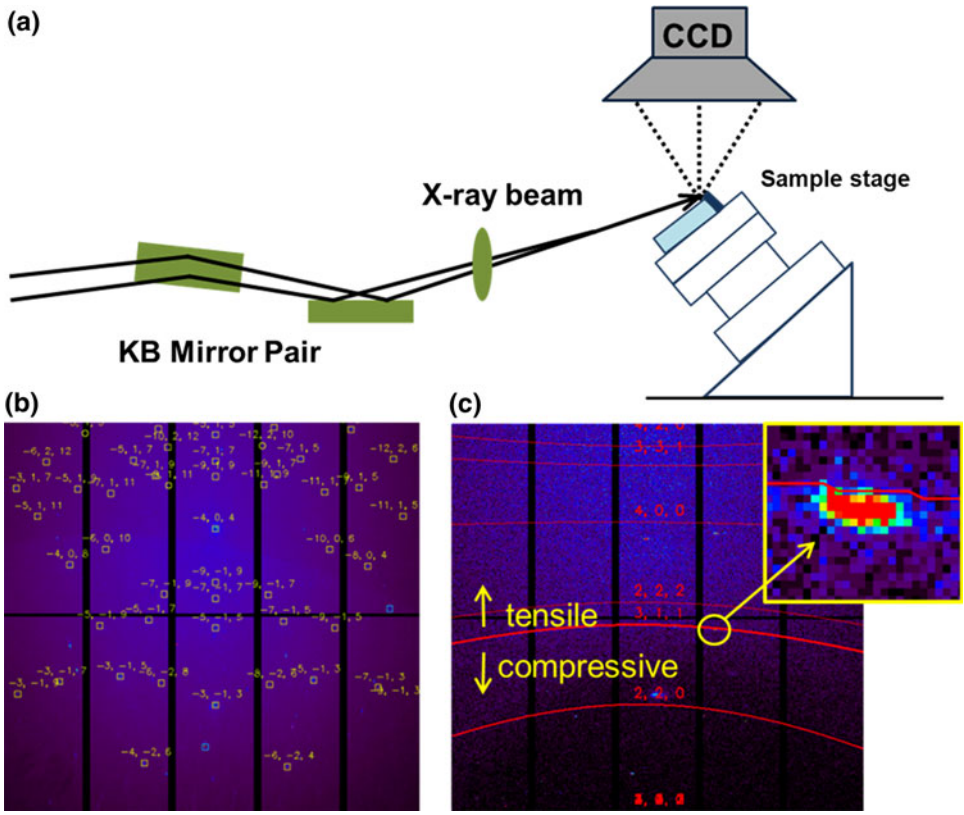

Fig. 1. White-beam and monochromatic-beam x-ray microdiffraction were used to study the submicron-scale local stress of TSV. (a) Schematic of synchrotron XRD at ALS, focused to submicron size by a KB mirror. (b) The deviatoric strain tensor is obtained from the Laue pattern by white-beam scanning. (c) The hydrostatic strain can be calculated from the peak positions in the Laue pattern.

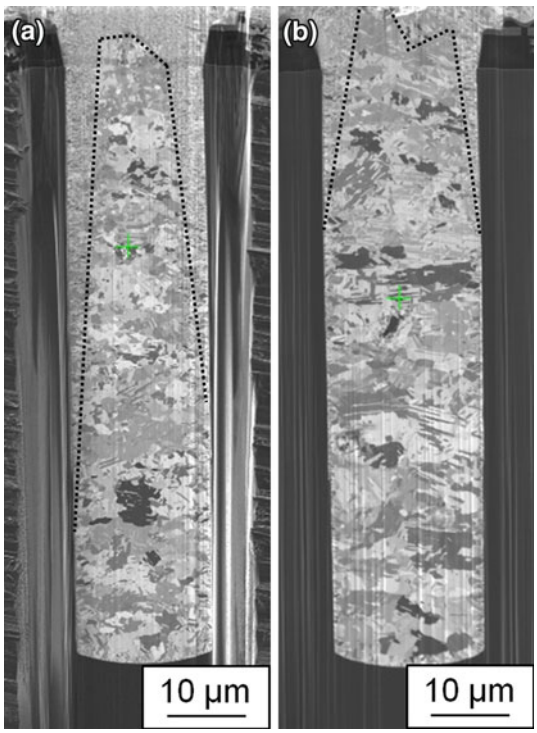

Fig. 2. FIB images of the TSV (a) before annealing and (b) after annealing at 200°C for 1 h. The small-grain area and the large-grain areas are indicated by the dotted line.

size of the Cu grains. In addition, abnormal grain growth and further growth of the large grains were not observed in the FIB image of the TSV after annealing.

Figure 3 shows EBSD images of the TSV and describes the results of the band contrast (BC), normal direction (ND), transverse direction (TD), and rolling direction (RD). The BC images show the relative intensity of the Kikuchi bands in the diffraction pattern. The grain boundaries and the grain structure of TSV were distinguished by dark lines without considering the texture of the Cu TSV. The textures of each Cu grain in the ND, TD, and RD images were described as being normal; however, the RD and TD are indistinguishable for EBSD analysis due to the cylindrical structure of the Cu TSV. Therefore, only the ND (vertical z-axis) is meaningful and is discussed herein. The inverse pole figures for before and after annealing TSV are shown in Fig. 4, and the percentages of (100), (110), and (111) textures are presented in Table I. All of the (100), (110), and (111) textures existed in less than 10% of the TSV sample both before annealing and after annealing, and no preferred orientation was observed. In Fig. 4, the intensity was statistically described by the multiple of uniform density (mud) with the maximum intensity of the contoured

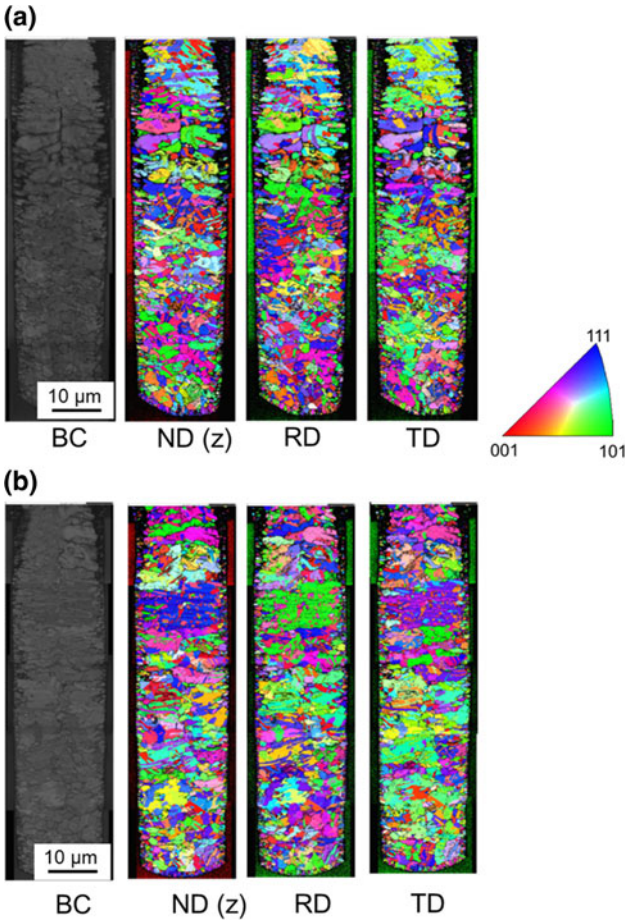

Fig. 3. EBSD orientation maps of the TSV (a) before annealing and (b) after annealing. Both of the TSVs had random orientation throughout the Cu TSV.

pole figures. A mud of 1 indicates randomly oriented grains,[21] and most of the values in Fig. 4 are below 1 mud. Therefore, Cu had a random texture both before annealing and after annealing the TSVs, as supported by Fig. 4. In addition, texture variation by annealing was not observed.

The grain size of the small grains and the large grains before and after annealing the TSVs are also presented in Table I. The grain sizes of the small grains, which were approximately 2.3 μm, did not change during the annealing process. In contrast, the sizes of the large grains increased after annealing, form 5.0 μm to 5.5 μm. This result indicates that the grain size in the center of the Cu TSV was only slightly altered and remained almost the same after annealing. These results correspond to the results of the FIB images taken before and after annealing the TSVs.

Figure 5 shows detailed FIB images of the TSV before annealing (Fig. 5b), after annealing (Fig. 5c), and after aging at room temperature (Fig. 5d). All the images show the same location as marked in Fig. 5a. To analyze the microstructure in the aged TSV, slight milling by FIB was performed on the same TSV sample before annealing for precise comparison of the microstructural changes caused by the aging effect. As shown by comparing the TSV before and after annealing with the FIB images shown in Fig. 5 and with the grain sizes calculated from the EBSD data in Table I, the large grains remained similar in grain size after annealing despite experiencing 200°C thermal loading for 1 h. Furthermore, additional room-temperature aging of the TSV showed both the small-grain and large-grain

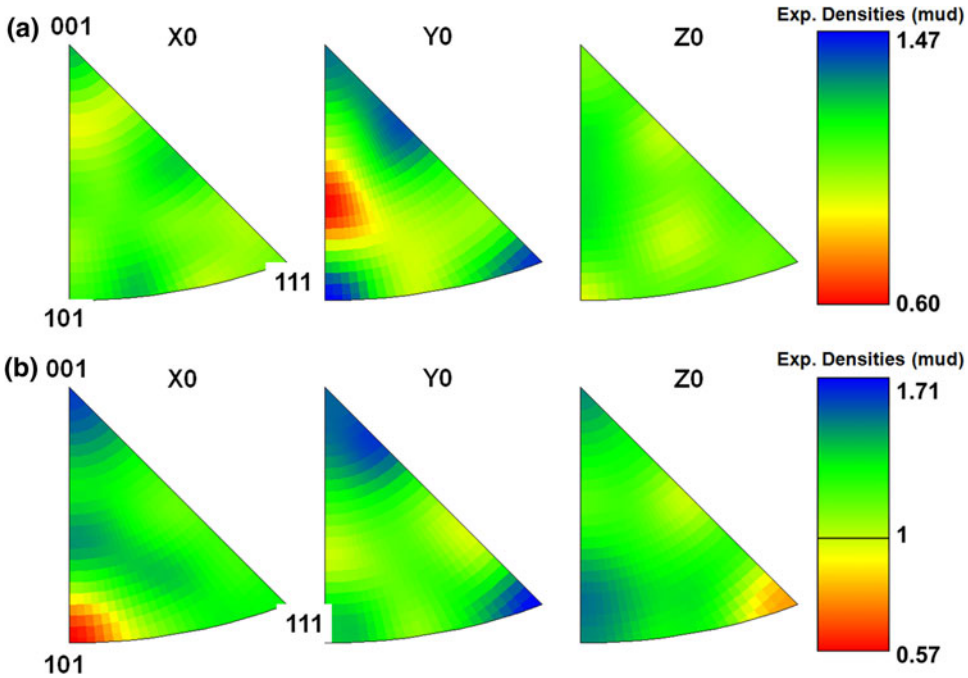

Fig. 4. Inverse pole figure images of TSV (a) before annealing and (b) after annealing with 12.5° half-width and 5° cluster size.

Table I. Percentage of (100), (110), and (111) texture and grain size of Cu at the small-grain area and the large-grain area in the as-received TSV and the TSV after annealing

	Texture			Grain Size	
	(100)	(110)	(111)	Fine-Grain Region	Large-Grain Region
Before annealing	5.0%	8.5%	7.5%	2.3 μm	5.0 μm
After annealing	5.2%	8.0%	9.6%	2.3 μm	5.5 μm

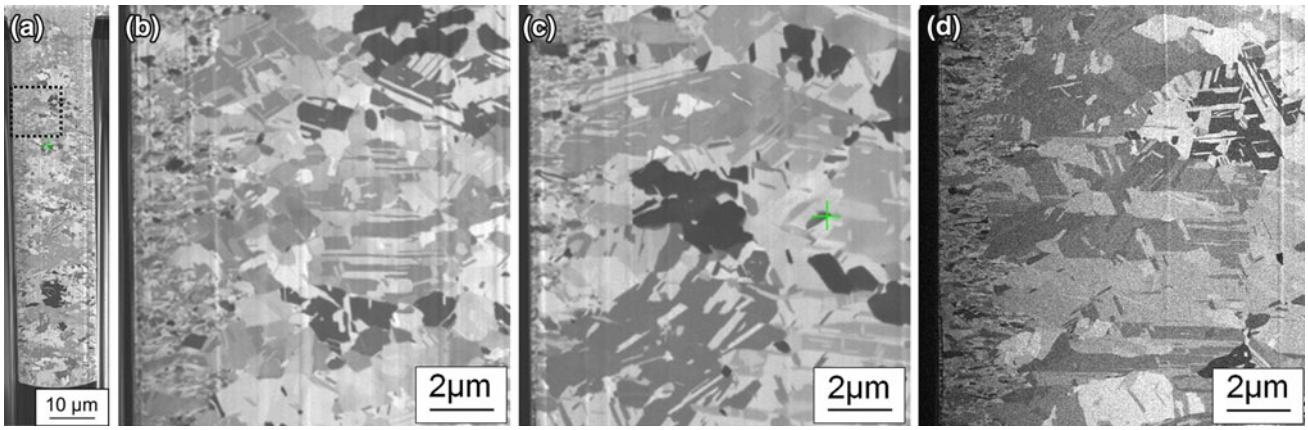

Fig. 5. (a) FIB image of the TSV with the closely investigated region highlighted. Enlarged FIB images of the TSV (b) before annealing, (c) after annealing at 200°C for 1 h, and (d) after aging at room temperature for 1 year.

regions, with unchanged ratio. These results contradict those of Okoro et al., who reported that the microstructure and grain size of the TSV changed with an increase in annealing conditions. For TSVs with 5 μm diameter and 23 μm depth, the maximum mean grain size of the as-deposited TSV was 1.6 μm, changing to 1.7 μm after room-temperature aging for 6 months. It changed to 2.3 μm after annealing at 300°C for 15 min and at 420°C for 20 min.[17]

The key point of differences for the restriction of microstructural change and the enlargement of grain size was due to the existence of twin boundaries in the Cu TSV. A result distinguishable from the EBSD measurements was a high proportion of twin boundaries. Figure 6a shows an EBSD image of the middle of the TSV before annealing. Twin boundaries were considered in this analysis. Twin boundaries are depicted by red lines, and the normal high-angle grain boundaries are illustrated by black lines. There are many twin boundaries in this EBSD image.

To quantify the twin boundaries in the EBSD data, the misorientation angle distribution (for the same part of the TSV) for Fig. 6a is shown in Fig. 6b. The 58.5° to 60° misorientation angles, representing first-order twin boundaries (Σ3 boundaries), represented a strikingly high proportion (28.5%) of all the misorientation angles. In addition, the second-order twin boundaries (Σ9 boundaries), which have an approximately 39.5° misorientation angle, accounted for 3.1%. The misorientation angle distribution was not the same for the normal random grain boundaries. These boundaries followed the Mackenzie plot, showing that twin boundaries accounted for a high proportion of the grain boundaries in the TSV. Considering all the parts of the TSV sample before annealing, the small-grain area accounted for 21.8% of the twin boundaries while the large-grain area accounted for 30.8%. Furthermore, after annealing, the TSV maintained its amount of twin boundaries. The small-grain area accounted for 21.2% of the twin boundaries, while the large-grain area accounted for 34.0%. This maintenance of the amount of twin boundaries also supports the effect of the twin boundaries on the restriction of the abrupt microstructure change of Cu in the TSV. Because twin boundaries are more stable than normal grain boundaries,[22] they prevent abnormal grain growth of Cu and contribute to maintenance of the grain size in the TSV. Regarding the effect of twin boundaries, it was reported that the grains in a copper film with many nanotwins grew only slightly after annealing at 200°C for 1 h, and many twin boundaries were still present in the sample after annealing. In contrast, grains in Cu film with few twins grew much more after annealing and showed abnormal grain growth after room-temperature aging for 1 year.[19] These phenomena indicate that twinned Cu grains are more stable to thermal annealing compared with Cu grains with few

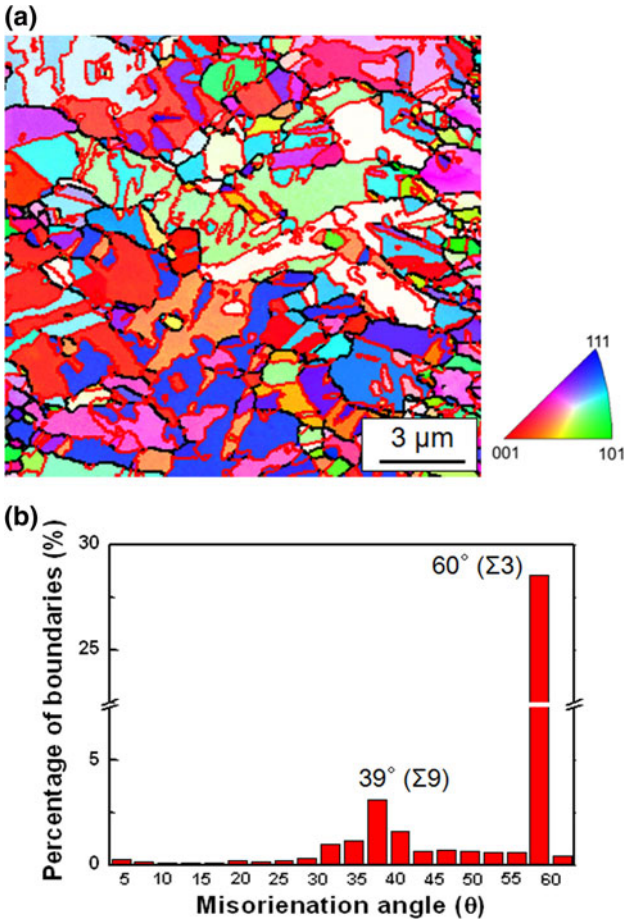

Fig. 6. (a) EBSD orientation map overlaid on the grain boundaries of the Cu TSV before annealing; black lines indicate high-angle grain boundaries, and red lines imply twin (Σ3) boundaries. (b) Misorientation angle distribution of the Cu TSV before annealing.

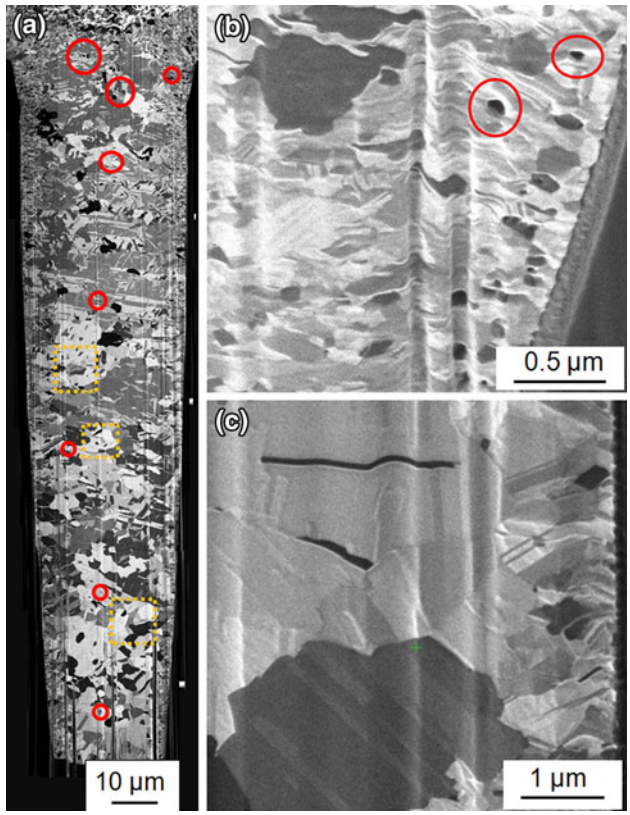

Fig. 7. Formation of voids and cracks after annealing: (a) locations of voids and cracks are marked, (b) voids formed in the top of TSV, and (c) cracks formed at the interface of the Cu grains in the right side of the TSV after annealing.

nanotwins. Twin boundaries inhibited the microstructural changes caused by annealing and aging.

Detailed analysis of the FIB images revealed that defects including microvoids and cracks were observed in the TSV after annealing, as shown in Fig. 7. The locations of the voids and crack are marked in Fig. 7a, and Fig. 7b shows an enlarged image of voids formed at the top side of the TSV. Figure 7c shows cracks formed at the right side in the bottom of a Cu TSV. Voids existed at the interface between the two grains, such as grain boundaries or twin boundaries, and some of the voids were formed at the region of grain size alteration in the top or side of the TSV as shown in Fig. 7b. In addition, cracks were observed in the inner part of the TSV. The formation of voids and cracks can be explained by the grain size deviation and induced stress in the Cu TSV. First, the inhomogeneous grain size distribution caused local deformation in the Cu due to its anisotropic properties as a function of temperature.[19] This local deformation, which occurred during annealing, induced the formation of defects, as shown in Fig. 7. In addition, the stress state of the TSV also caused the formation of defects.

The average hydrostatic stress of the Cu TSV before annealing was 229 MPa. All the stress tensors for the TSV before annealing were mapped and are illustrated in Fig. 8. These stress tensors were summed with the hydrostatic stress and the deviatoric stress components. The normal stress components (σ_{xx}, σ_{yy}, and σ_{zz}) represent the sum of the hydrostatic stress and deviatoric stress for each position, and the shear stress components (σ_{xy}, σ_{yz}, and σ_{xz}) represent the deviatoric stress. The TSV sample that did not receive any post-treatment had tensile hydrostatic stress. Tensile stress developed due to residual stress from fabrication and grain growth after deposition because the TSV should maintain its shape (cylindrical structure) and coherent connection with surrounding materials, regardless of microstructural changes. In addition, all the stress components had locally high compressive or high tensile values with large deviation among stresses in the TSV before annealing. These deviations were induced by the large gap of grain sizes between the inner and outer part of the TSV, as shown in Figs. 2 and 5. Regarding the effect of stress on defect formation, thermal stress was induced differently among grains or between the twin

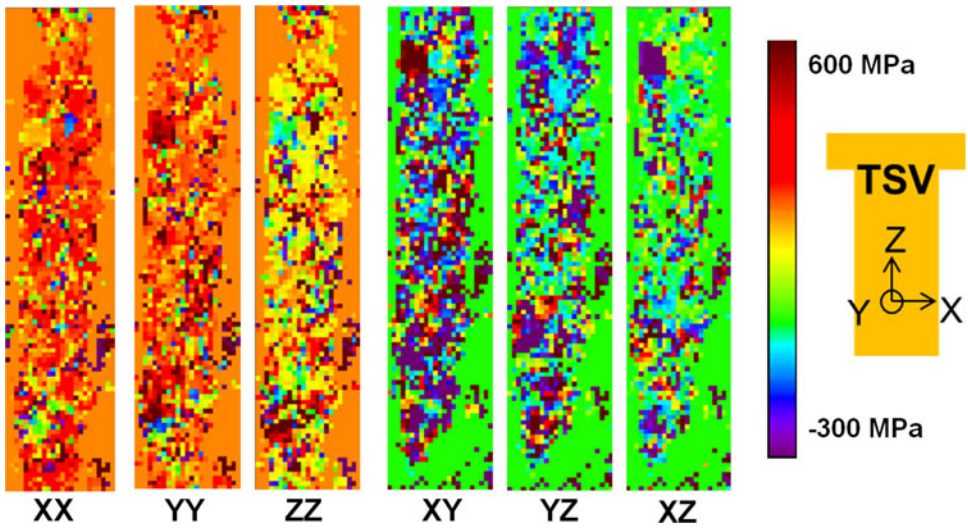

Fig. 8. Stress maps of the Cu TSV with all the stress tensors for the TSV before annealing.

phase and the parent phase during thermal annealing due to the different orientation of the sample[23] because Cu is an anisotropic material. A stress difference may cause stress concentration at the interfaces, corners, and intersections of Cu grains, and this effect of stress concentration may cause the formation of voids and cracks in the stress-concentrated sites shown in Fig. 8a, b. In addition, the hydrostatic stress was 177 MPa after thermal annealing. Our group previously reported the stress and its profile in TSVs before, during, and after annealing.[24] The hydrostatic stress remained tensile because additional grain growth and the microstructural change of large grains were restricted by the twin boundaries, as discussed above. However, the level of stress in the TSV after annealing was decreased by the formation of defects in the TSV.

CONCLUSIONS

The microstructural evolution of a Cu TSV on thermal annealing was investigated in this work. The Cu TSV had two microstructural sections with different grain size. Both had a random texture both before and after annealing. The grain size of the inner part of the TSV was larger than at the top and the edge of the TSV, and the grain sizes of large grains was almost the same for the TSV before and after annealing. The maintenance of the microstructure in the Cu TSV was affected by its boundary characteristics. The TSV contained many twin boundaries, and these stable boundaries restricted grain growth during annealing and additional aging. However, microvoids and cracks were formed in the TSV after thermal annealing due to its grain size deviation and stress concentration on annealing. These defects reduced the local stress in the TSV after annealing. Understanding microstructural evolution and its effect on stress in TSVs can enable the prediction of the effects of TSV fabrication and 3-D integration reliability.

ACKNOWLEDGEMENTS

This project was conducted through the Practical Application Project of Advanced Microsystems Packaging Program of Seoul Technopark, funded by the Ministry of Knowledge Economy (10029790). The Advanced Light Source is supported by the Director, Office of Science, Office of Basic Energy Sciences, Materials Sciences Division, of the US Department of Energy under Contract No. DE-AC02-05CH11231 at Lawrence Berkeley Nationalz Laboratory and University of California, Berkeley, CA. The move of the microdiffraction program from ALS beamline 7.3.3 onto to the ALS superbend source 12.3.2 was enabled through NSF Grant No. 0416243. One of the authors (A.S.B.) is supported by the Director, Los Alamos National Laboratory (LANL), under the Los Alamos National Laboratory Director's Postdoctoral Research Fellowship program (LDRD/X93V).

REFERENCES

1. D.J. Frank, R.H. Dennard, E. Nowak, P.M. Solomon, Y. Taur, and H.S.P. Wong, *Proc. IEEE* 89, 259 (2001).
2. J.D. Meindl and J.A. Davis, *IEEE J. Solid State Circuits* 35, 1515 (2000).
3. L. Xue, C.C. Liu, H.S. Kim, S. Kim, and S. Tiwary, *IEEE Trans. Electron Dev.* 50, 601 (2003).
4. R. Reif, A. Fan, K.-N. Chen, and S. Das, *Proc. International Symposium on Quality Electronic Design (ISQED)* (2002), p. 33.
5. X. Wu, P.C.-H. Chan, S. Zhang, C. Feng, and M. Chan, *IEEE Trans. Electron Dev.* 52, 1998 (2005).
6. A. Rahman, A. Fan, J. Chung, and R. Reif, *IEEE International Interconnect Technology Conference* (2000), p. 18.
7. S.J. Souri and K.C. Saraswat, *1999 IEEE International Interconnect Technology Conference* (1999), p. 24.
8. K.W. Lee, T. Nakamura, T. Ono, Y. Yamada, T. Mizukusa, K.T. Park, H. Kurino, and M. Koyanagi, *Dig. Int'l Elect. Dev. Meeting* (2000), p. 165.

9. C. Okoro, Y. Yang, B. Vandevelde, B. Swinnen, D. Vandepitte, B. Verlinden, and I. De Wolf, *IEEE International Interconnect Technology Conference* (2008).
10. X. Liu, Q. Chen, P. Dixit, R. Chatterjee, R.R. Tummala, and S.K. Sitaraman, *Electronic Components and Technology Conference* (2009).
11. P. Dixit, S. Yaofeng, J. Miao, J.H.L. Pang, R. Chatterjee, and R.R. Tummalaa, *J. Electrochem. Soc.* 155, H981 (2008).
12. I.U. Abhulimen, A. Kamto, Y. Liu, S.L. Burkett, and L. Schaper, *J. Vac. Sci. Technol. B* 26, 1834 (2008).
13. M.J. Wolf, T. Dretschkow, B. Wunderle, N. Jürgensen, G. Engelmann, O. Ehrmann, A. Uhlig, B. Michel, and H. Reichl, *Electronic Components and Technology Conference* (2008).
14. Nay. Lin, Jianmin. Miao, and Pradeep. Dixitb, *J. Electrochem. Soc.* 157, D323 (2010).
15. A. Radisic, O. Lühn, H.G.G. Philipsen, Z. El-Mekki, M. Honore, S. Rodet, S. Armini, C. Drijbooms, H. Bender, and W. Ruythooren, *Microelectron. Eng.* 88, 701 (2011).
16. C. Huyghebaert, J. Van Olmen, O. Chukwudi, J. Coenen, A. Jourdain, M. Van Cauwenberghe, R. Agarwahl, A. Phommahaxay, M. Stucchi, and P. Soussan, *Electronic Components and Technology Conference* (2010).
17. C. Okoro, K. Vanstreels, R. Labie, O. Lühn, B. Vandevelde, B. Verlinden, and D. Vandepitte, *J. Micromech. Microeng.* 20, 045032 (2010).
18. M. Kunz, N. Tamura, K. Chen, A.A. MacDowell, R.S. Celestre, M.M. Church, S. Fakra, E.E. Domning, J.M. Glossinger, J.L. Kirschman, G.Y. Morrison, D.W. Plate, B.V. Smith, T. Warwick, V.V. Yashchuk, H.A. Padmore, and E. Ustundag, *Rev. Sci. Instrum.* 80, 035108 (2009).
19. D. Xu, H.-P. Chen, and K.N. Tu, *Stress-Induced Phenomena in Metallization: 11th International Workshop* (2010).
20. A. Radisic, O. Lühn, H.G.G. Philipsen, Z. El-Mekki, M. Honore, S. Rodet, S. Armini, C. Drijbooms, H. Bender, and W. Ruythooren, *Microelectron. Eng.* 88, 701 (2010).
21. P.A. Bland, L.E. Howard, D.J. Prior, J. Wheeler, R.M. Hough, and K.A. Dyl, *Nat. Geosci.* 4, 244 (2011).
22. O. Anderoglu, A. Misra, H. Wang, and X. Zhang, *J. Appl. Phys.* 103, 094322 (2008).
23. A. Sekiguchi, S. Kamiya, M. Saka, K. Maruyama, and J. Koike, *Appl. Phys. Lett.* 79, 27 (2001).
24. A.S. Budiman, H.-A.-S. Shin, B.-J. Kim, S.-H. Hwang, H.-Y. Son, M.-S. Suh, Q.-H. Chung, K.-Y. Byun, N. Tamura, M. Kunz, and Y.-C. Joo, *Microelectron. Reliab*. (2011).